COMET C/2011 J2 (LINEAR) NUCLEUS SPLITTING: DYNAMICAL AND STRUCTURAL ANALYSIS

Federico Manzini [ax], Virginio Oldani [a], Masatoshi Hirabayashi [b], Raoul Behrend [c], Roberto Crippa [a], Paolo Ochner [d], José Pablo Navarro Pina [e], Roberto Haver [f], Alexander Baransky [g], Eric Bryssinck [h], Andras Dan [a], Josè De Queiroz [i], Eric Frappa [m], Maylis Lavayssiere [n]

[a] Stazione Astronomica – Stazione Astronomica di Sozzago, 28060 Sozzago (Italy) and FOAM13, Osservatorio di Tradate, Tradate (Italy)

[ax] Corresponding author; e-mail address: manzini.ff@aruba.it

[b] M. Hirabayashi, Earth, Atmospheric and Planetary Science, Purdue University, West Lafayette, IN 47907-2051 (USA)

[c] R. Behrend, Geneva Observatory, Geneva (Switzerland)

[d] P. Ochner, INAF Astronomical Observatory of Padova (Italy)

[e] J. P. Navarro Pina, Asociacion Astronomica de Mula (Murcia, Spain)

[f] R. Haver, Osservatorio di Frasso Sabino (Italy)

[g] A. Baransky, Astronomical Observatory of Kyiv University (Ukraine)

[h] E. Bryssinck, BRIXIIS Observatory, Kruibeke (Belgium)

[i] J. De Queiroz, Sternwarte Mirasteilas, Falera (Switzerland)

[m] E. Frappa, Saint-Etienne Planetarium (France)

[n] M. Lavayssiere, Observatoire de Dax (France)

Correspondence to:
Dr. Federico Manzini
Stazione Astronomica
Cascina Guascona
28060 Sozzago (Novara) – Italy
e-mail: manzini.ff@aruba.it
Ph.: +39 3408077664

ABSTRACT

After the discovery of the breakup event of Oort cloud comet C/2011 J2 in August 2014, we followed the primary body and the main fragment B for about 120 days in the context of a wide international collaboration.
From the analysis of all published magnitude estimates we calculated the comet's absolute magnitude H=10.4, and its photometric index n=1.7. We also calculated a water production of only 110 kg/s at the perihelion. These values are typical of a low-activity, long-period or new comet.
Analysis of the motion of fragment B over the observation period showed that the first breakout event likely occurred between 12 July and 30 July 2014. Nucleus B remained persistently visible throughout the 4-month observation period.
The projected separation velocity of nucleus B from the parent body was 4.22 m/s at the time of the breakup and 12.7 m/s at the end of the observation period, suggesting that nucleus B was subjected to a constant deceleration $a = 6.87 \cdot 10^{-7} m/s^2$.
The spin period of the main nucleus was estimated as 4.56h ± 0.05h by photometric analysis.
The structural analysis of the comet showed that a cohesive strength of the nucleus greater than ~0.9 kPa; assuming a bulk density of 500 kg/m^3, with a rotation period of 4.56h the cometary nucleus may fail structurally, especially if the body is elongated.
These results suggest that the nucleus of comet C/2011 J2 may have an elongated shape, with a ratio of the semi-minor axis to the semi-major axis $\beta < 0.675$; the semi-major axis of the pristine nucleus should be larger than 8 km.
From this study, we propose that rotational disruption, possibly combined with sublimation pressure, was a reasonable explanation for the breakup event in comet C/2011 J2.

Keywords: Comets; comet C/2011 J2 (LINEAR); spin axis; rotation; break-up.

1 INTRODUCTION

Progressive fragmentation is one of the main events leading to complete disintegration of cometary nuclei and to their extinction (*Sekanina, 1982, 2005*).
In the case of comets that closely approach the Sun, fragmentation is often preceded by significant nucleus erosion, and may be associated with activity outbursts, with appearance of inner coma features (*Sekanina, 2002*). However, although some objects such as 133P/Elst-Pizarro (*Hsieh et al., 2010*) may show similar activities, this is not usually the case for more distant comets that are considered to be less influenced by solar radiation. Evidence of nucleus splitting in such cases is usually provided through the detection of one or more secondary components (a fragment or companion) arising from the same parent body and usually moving in close orbits.

Several fragmentation mechanisms have been proposed to explain splitting of cometary nuclei: tidal disruption, rotational forces, thermal stress, internal gas pressure and impacts by other solar system bodies (*Altenhoff, 2009; Boehnhardt, 2004*). However, while tidal disruption has been generally accepted as the most likely mechanism for the splitting of comet P/Shoemaker-Levy 9 (*Weaver, 1997*) and 16P/Brooks 2 (*Sekanina, 1985*), none of the other scenarios were ideally detected.
This may come from the fact that the most important parameters of cometary nuclei (such as internal structure, size and rotation) used in these models were not well known, and the available observations did not allow to ascertain the actual sequence of events, as most of the secondary components of a split comet vanish with time, or become too faint to be detected even with the largest telescopes.

In this paper we study comet C/2011 J2 (LINEAR), which has recently incurred multiple splitting events at a considerable distance from the Sun (r > 4 AU). This event appeared very interesting, as at this distance no significant heating from solar radiation is expected, such as to trigger phenomena that could lead to a fragmentation of the nucleus.
Given the scarcity of data in the literature on the fragmentation of distant comets, we investigated the multiple fragmentation of this comet and the evolution of the companion nuclei over the first months following the first breakup event, with the aim of better understanding the possible causes that could have led to the detachment of the fragments and to identify the physical parameters typical of this cometary nucleus.

2 COMET C/2011 J2 (LINEAR): DISCOVERY AND EVOLUTION OF ITS FRAGMENTATION

2.1 Description of discovery of the comet

Comet C/2011 J2 is an Oort cloud comet that was discovered on 4 May 2011 by M. Blythe, G. Spitz, R. Brungard, J. Paige, P. Festler, T. McVey, and A. Valdivia with the LINEAR 1-meter f/2.15 reflector (*Williams, 2011)*. It brightened at an apparent magnitude of 19.7 at the time of discovery.

This comet was successively found on earlier images taken on 10 and 25 March 2011 with the Catalina Sky Survey 0.68-m Schmidt camera by A.D. Grauer et al. (*Williams, 2011*).

C/2011 J2 was dynamically new. The orbit of this comet is almost parabolic, with an eccentricity of 1.00051; it came to perihelion on 25 December 2013 at a distance of 3.4 AU from the Sun. There are no reports that provide particular phenomena related to this comet after its discovery.

2.2 Description of discovery of fragmentation

On 27 August 2014 a 18th magnitude fragment was detected by F. Manzini, V. Oldani, A. Dan, R. Crippa and R. Behrend with the 0.4 m reflector at the SAS Observatory 0.8” east and 7.5” north of the main, brighter nuclear condensation (*Green, 2014*) (**Figure 1**).

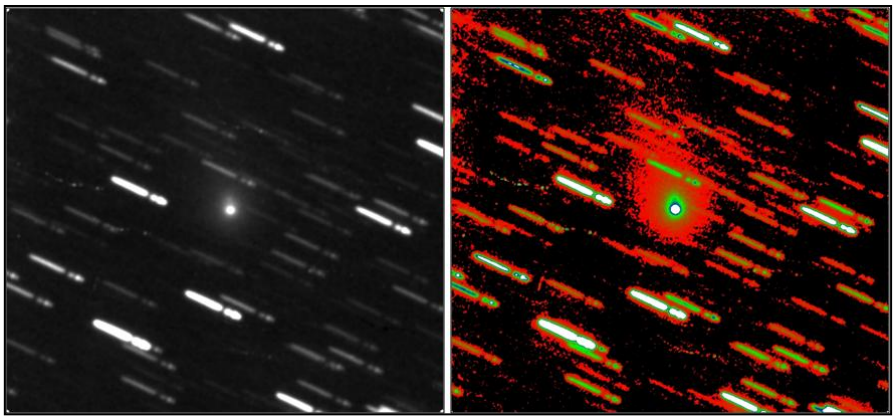

Figure 1. Discovery of the splitting of comet C/2011 J2

Astrometry of the main nucleus and of the secondary component was reported in preliminary studies (*Green, 2014*; *Williams, 2014c, 2014d,2014e; Spahr, 2014*). The secondary component was named C/2011 J2-B.

At the time of discovery of the fragmentation, the comet was at a distance of 4.1 AU from the Sun. The coma of the main nucleus looked evenly circular, with a diameter of 50" (about 90,000 km). The projected distance between the two nuclei was about 20,000 km on the plane of the sky, and a relative motion was detected only after several days of observation. These findings suggested that the comet splitting had occurred several weeks before the date of discovery.

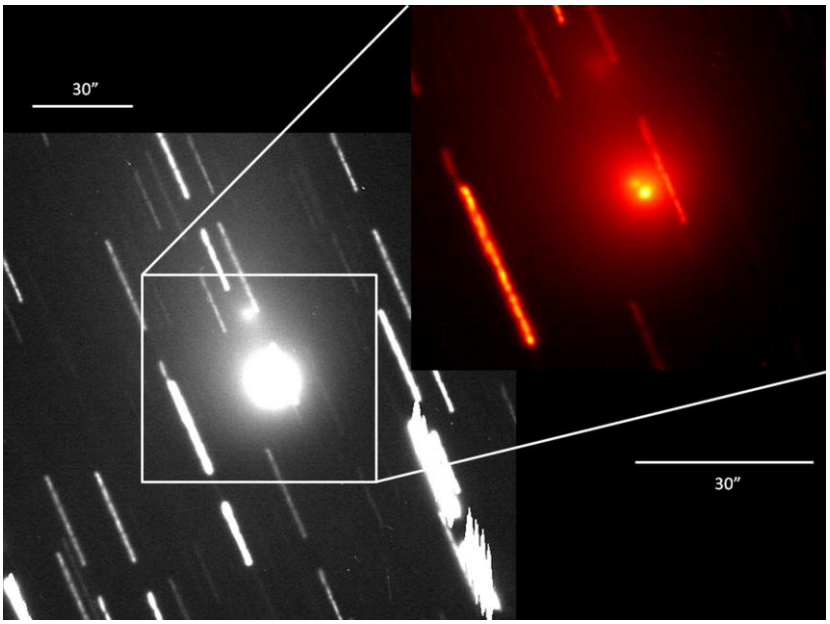

Figure 2. Enhancement of coma details

A second fragmentation was observed on 4.9 October 2014 by *E. Guido, N. Howes,* and *M. Nicolini* on images taken with the 2.0-m Liverpool telescope at La Palma (*Williams, 2014f*). This third component was named C/2001 J2-C (**Figure 2**).

3 METHODS

We followed comet C/2011 J2 from 27 August 2014, the date of discovery of the fragmentation, until 11 December 2014; two additional images of the comet, taken prior to the discovery of the splitting and in which the fragment was already detectable, were successively retrieved. In total, the observations span over a period of 121 days.

Observations of comet C/2011 J2 (Linear): Observatories and CCD

Code	Observatory	Sensor	Resolution arcsec/px	Country	Telescope	Filters
IAU 157	**Frasso Sabino**	KAF-1301E	1.31	Italy	SCT 0.37m	broadband
IAU 209	**Asiago Astrophysical Obs.**	E2V CCD42-40	0.52	Italy	Reflector 1.82m	SDSS R
IAU 209	**Asiago Astrophysical Obs.**	KAI-11000M	0.86	Italy	Schmidt 67/91cm	R
IAU 585	**Kyiv Comet Station**	E2V CCD47-10	0.95	Ukraine	AZT-8 refl. 0.7m	R
IAU 586	**Pic du Midi**	Marconi DZ936BV	0.21	France	Reflector 1.05m	R
IAU A12	**Stazione Astr. Sozzago (SAS)**	KAF-1603ME	0.69	Italy	Cassegrain 0.4m	200 nm broadband, center at 650 nm
IAU B13	**FOAM13**	KAF-1603ME	0.57	Italy	Reflector 0.65m	200 nm broadband, center at 650 nm
IAU B96	**BRIXIIS**	KAF-6303E	1.26	Belgium	Reflector 0.4 m	broadband
IAU F65	**Faulkes N, LCGOT**	FI CCD486	0.3	Hawaii, USA	Reflector 2m	Bessell R'
IAU J13	**Liverpool Tel.**	E2V CCD231-84-5-E24	0.3	La Palma, Spain	Reflector 2m	SDSS R
TNG	**Telescopio Nazionale Galileo (N28.7539°, W17.8931°)**	E2V CCD42-40	0.25	La Palma, Spain	Reflector 3.58m	SDSS G, SDSS R

Table 1

The images were taken at several different observatories with telescopes having a spatial resolution between 0.57 and 1.23 arcsec/pixel **(*Table 1*).** This resolution is optimal to investigate the morphology of the area near the nucleus, as shown in previous studies that had been successfully carried out on comets Hyakutake (C/1996 B2), Hale-Bopp (C/1995 O1) (*Manzini et al., 2001, Schwarz et al., 1997*), Ikeya-Zhang (C/2002 C1) (*Manzini et al., 2007*), Machholz (C/2004 Q2) (*Manzini et al., 2011*) and McNaught (260P/2012 K2) (*Manzini et al., 2014*).

In addition, high-resolution images (between 0.21 and 0.3 arcsec/pixel) were obtained from larger telescopes, either taken directly (Pic du Midi, France; Telescopio Nazionale Galileo, Canary Islands) or retrieved from public websites (Faulkes North, Haleakala, Hawaii; Liverpool telescope, Canary Islands).

Although most of the images were taken at few observatories located in Italy, the data published in this paper are thus the result of a wide international *pro-am* collaboration. The full list of the images used in this study, by date and with full description of their characteristics, is shown in ***Table 2***.

Images of Comet C/2011 J2 Linear

Date	Mean time UT	Observ.	N of images during obs. sessions	Filters	Tot. Exp. (s)	Scale ("/pix)	Scale (km/pix)	Δ (AU)	R (AU)	Phase angle (°)
2014-04-02	18.30	IAU 585	12	R	660	0,95	2857	4,149	3,562	12
2014-06-11	22.30	IAU B96	8	clear	960	1,26	3920	4,292	3,776	12,5
2014-06-14	23.30	IAU B96	7	clear	840	1,26	3903	4,274	3,788	12,7
2014-07-01	23.30	IAU B96	6	clear	720	1,26	3786	4,146	3,854	14
2014-08-17	22.30	IAU 157	5	clear	450	1,31	3488	3,674	4,060	13,9
2014-08-19	19.30	IAU 585	14	R	840	0,95	2519	3,658	4,069	13,8
2014-08-20	23.30	IAU B96	7	clear	840	1,26	3331	3,647	4,074	13,7
2014-08-26	01.30	IAU 585	8	R	420	0,95	2482	3,605	4,099	13,2
2014-08-27	23.30	IAU A12	20	broad R	2340	0,68	1769	3,590	4,108	13
2014-08-28	23.30	IAU A12	20	broad R	3300	0,68	1766	3,583	4,113	12,9
2014-08-30	23.30	IAU A12	23	broad R	2100	0,68	1759	3,569	4,122	12,6
2014-09-02	23.30	IAU A12	45	broad R	7920	0,68	1750	3,550	4,137	12,3
2014-09-02	23.30	IAU B13	93	broad R	5580	0,57	1467	3,550	4,137	12,3
2014-09-03	15.20	IAU F65	22	R	685	0,30	771	3,545	4,141	12,2
2014-09-04	00.30	IAU 586	48	R	2880	0,21	539	3,544	4,142	12,2
2014-09-04	10.30	IAU F65	11	R	500	0,30	770	3,540	4,145	12,1
2014-09-13	23.00	IAU A12	23	broad R	3060	0,68	1725	3,499	4,192	10,9
2014-09-16	23.00	IAU A12	17	broad R	2700	0,68	1721	3,492	4,507	10,6
2014-09-17	00.30	IAU B96	57	clear	1800	1,26	3191	3,494	4,202	10,7
2014-09-17	01.00	IAU 585	12	R	300	0,95	2404	3,492	4,207	10,6
2014-09-21	21.30	IAU A12	21	broad R	2520	0,68	1719	3,487	4,232	10
2014-09-22	18.30	IAU 209	8	R,G	1200	0,86	2174	3,487	4,242	9,9
2014-09-23	23.00	IAU A12	27	broad R	4740	0,68	1719	3,487	4,242	9,9
2014-09-23	19.10	IAU 209	10	R	3000	0,86	2174	3,487	4,242	9,9
2014-09-26	21.00	IAU 209	4	R	900	0,86	2175	3,490	4,258	9,6
2014-09-26	23.30	IAU J13	10	R	2000	0,30	759	3,491	4,258	9,6
2014-09-27	23.30	IAU B13	30	broad R	1740	0,57	1443	3,492	4,263	9,6
2014-09-27	02.30	IAU 585	12	R	360	0,86	2177	3,492	4,259	9,6
2014-09-27	20.30	IAU B96	41	clear	2460	1,26	3189	3,492	4,261	9,6
2014-09-28	23.30	IAU B13	120	broad R	7200	0,57	1443	3,494	4,268	9,4
2014-09-29	22.30	IAU B13	140	broad R	8340	0,57	1444	3,495	4,269	9,4
2014-09-29	21.30	IAU A12	52	broad R	6600	0,68	1723	3,495	4,269	9,4
2014-09-29	02.30	IAU 585	12	R	360	0,95	2407	3,495	4,269	9,4
2014-10-01	11.00	IAU F65	18	R	540	0,30	761	3,502	4,281	9,3
2014-10-02	22.20	IAU F65	18	R	540	0,30	762	3,505	4,287	9,2
2014-10-03	23.50	IAU 585	19	R	1440	0,95	2418	3,512	4,294	9,2
2014-10-10	23.50	IAU 585	13	R	780	0,95	2445	3,551	4,331	9,1
2014-10-12	21.20	IAU 585	13	R	780	0,95	2455	3,565	4,342	9,1
2014-10-13	22.20	IAU A12	14	broad R	1620	0,68	1761	3,573	4,347	9,2
2014-10-14	23.20	IAU 585	13	R	780	0,95	2466	3,582	4,352	9,2
2014-10-17	22.20	IAU B13	87	broad R	4920	0,57	1491	3,609	4,368	9,3
2014-10-17	22.20	IAU A12	45	broad R	4800	0,68	1779	3,609	4,368	9,3
2014-10-18	23.20	IAU B13	154	broad R	9240	0,57	1495	3,618	4,373	9,4
2014-10-18	22.20	IAU A12	50	broad R	4560	0,68	1783	3,618	4,373	9,4
2014-10-24	01.00	IAU 585	25	R	900	0,95	2530	3,675	4,401	9,7
2014-10-25	12.00	TNG	12	R,G	1500	0,25	670	3,698	4,411	9,8
2014-10-30	18.10	IAU 209	6	R	2100	0,86	2347	3,765	4,438	10,2
2014-11-01	22.10	IAU 209	31	R	8400	0,86	2365	3,794	4,449	10,4
2014-11-01	18.30	IAU A12	17	broad R	1000	0,68	1870	3,794	4,449	10,4
2014-11-02	19.30	IAU 209	24	B,R	3600	0,52	1436	3,809	4,455	10,5
2014-11-05	21.00	IAU 585	15	R	900	0,95	2656	3,857	4,472	10,7
2014-11-13	18.30	IAU A12	10	broad R	1200	0,68	1968	3,993	4,516	11,4
2014-11-20	19.00	IAU A12	25	broad R	1680	0,68	2033	4,125	5,071	11,8
2014-11-20	19.00	IAU 209	16	R	4200	0,86	2571	4,125	5,071	11,8
2014-11-21	22.30	IAU 585	20	R	1200	0,95	2855	4,146	4,561	11,8
2014-11-23	19.00	IAU A12	30	broad R	4200	0,68	2063	4,185	4,572	11,9
2014-11-24	22.30	IAU 209	12	R	3600	0,86	2622	4,206	4,577	12,0
2014-12-11	18.30	IAU 209	48	R	14400	0,86	2853	4,577	4,679	12,1
2014-12-12	20.30	IAU A12	110	broad R	7800	0,68	2263	4,592	4,681	12,1
2014-12-12	21.30	IAU 209	6	R	1800	0,86	2862	4,592	4,681	12,1
2014-12-17	05.40	IAU F65	10	R	350	0,30	1019	4,688	4,706	12,0
2014-12-18	06.40	IAU F65	10	R	750	0,30	1024	4,711	4,711	12,0
2014-12-25	19.00	IAU A12	63	broad R	7560	0,68	2406	4,881	4,756	11,6
2015-01-05	19.00	IAU A12	53	broad R	4920	0,68	2524	5,122	4,821	10,8
2015-09-06	23.30	IAU A12	104	broad R	9720	0,68	2649	5,374	6,366	1,8
2015-09-07	01.30	IAU 209	16	R	4800	0,86	3350	5,375	6,366	1,8
2015-09-08	23.30	IAU B13	160	broad R	9660	1,04	4058	5,384	6,379	1,6
2015-09-09	00.30	IAU A12	53	broad R	6300	0,68	2654	5,384	6,379	1,6
2015-09-19	01.00	IAU B13	200	broad R	12000	1,04	4114	5,458	6,445	1,8
2015-09-21	00.30	IAU B13	200	broad R	12000	1,04	4128	5,477	6,459	2,1
2015-09-21	22.30	IAU B13	200	broad R	12000	1,04	4135	5,486	6,464	2,2

Table 2

Each filtered or unfiltered CCD image was first calibrated by means of conventional methods (bias, dark and flat-field images, collected as required by the procedures of each observatory on the same night of the observing sessions). Subsequently, any further processing was applied to the sum of series of images taken on the same night, rather than on each single shot, after registering at a sub-pixel level the single frames to a common center (the brightest peak of the optocenter), to increase the S/N ratio. The time lag between the first and last co-added images was generally lower than 40 min.

Additional processing was performed by means of the Larson-Sekanina spatial filter (*Larson and Sekanina, 1984*) to highlight radial features (i.e. jets) and haloes (i.e. shells) if presents around the cometary nucleus. Many details have been drawn using a filter that applies a radial gradient centered on the brightest peak of

the optocenter. This filter creates an artificial coma, based on the photometry of the original image, then divides the original image itself in order to highlight the presence of different brightness levels in the inner coma very close to the nucleus, which would normally be hidden by the diffuse glow of the coma (*Manzini et al., 2014*)(**Figure 3**).

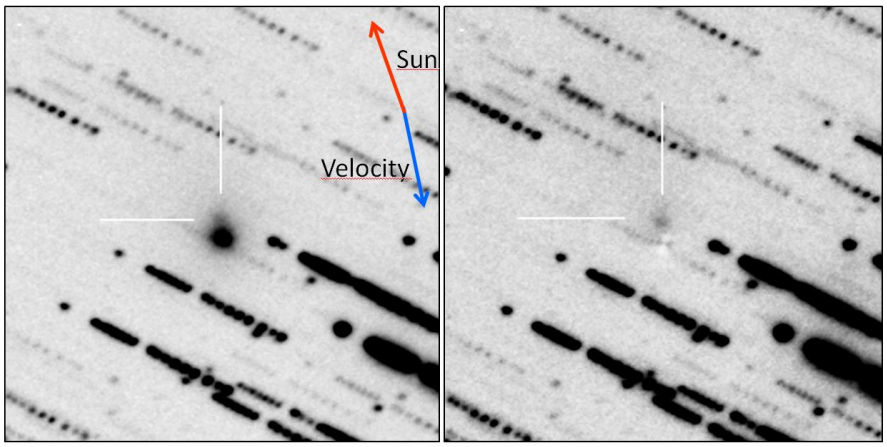

Figure 3. Enhancement of details: radial gradient filter

3.1 Distance and Position Angle

The distance between the primary nucleus and the secondary body B, as well as the position angle of the latter relative to the first, were determined with the highest precision by performing the following procedures:

- first, the images were re-sampled 2x in both axes to increase the accuracy of the measurements;
- second, a radial gradient filter was applied centered on the main nucleus, and the original image was divided by the filtered one to "hide" the coma of the main nucleus and to better distinguish the secondary body (**Figure 3**);
- finally, the resulting image was submitted to polar coordinates transformation centered on the optocenter position of the primary body, with a resolution of 0.5°/pixel on the horizontal axis (corresponding to the θ angle), and a resolution of 1 pixel on the vertical axis.

A first photometric profile was drawn parallel to the horizontal axis and crossing the bright area corresponding to nucleus B, to precisely identify the position of its optocenter (in correspondence of the peak of brightness). The *Position Angle* (PA) between the primary nucleus and the secondary body B was precisely measured for each of the observation dates by reading the exact x-axis coordinate of the peak of brightness corresponding to the optocenter of nucleus B, and halving the measured value to the original resolution. The estimated error was less than ±1° (**Figure 4**). The measured PAs were then converted assuming north to be at zero degrees and read counterclockwise, and plotted against time and against the related distance between the two bodies, in order to detect any possible relative orbital motion of them.

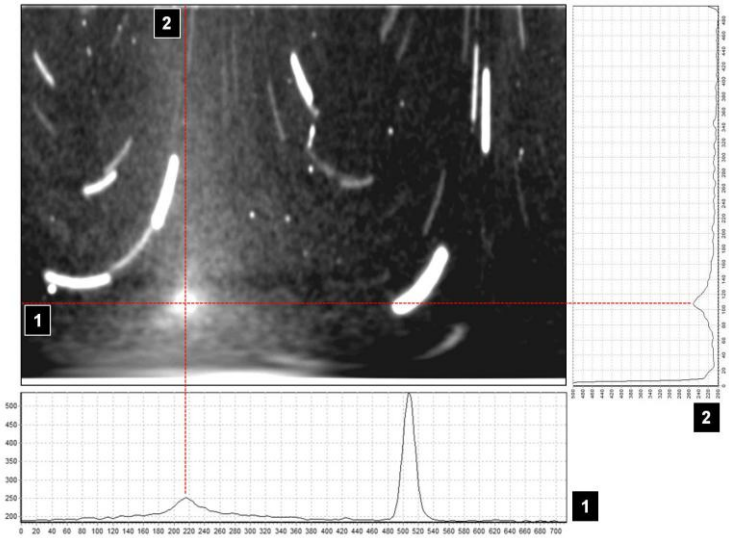

Figure 4. Measurement method of the positions of nucleus B

A second profile was then drawn orthogonally to the first across the optocenter of nucleus B identified as before. The *distance* in pixels between the two bodies was measured (with an estimated error of max ± 2 pixels) as the separation between the x-axis (i.e. the optocenter of the main nucleus) and the optocenter of nucleus B (**Figure 4**). The obtained value was halved, converted to angular separation in arcsecs according to the image resolution, normalized according to the actual distance from the Earth for the given date, and finally changed into kilometers. The data have then been plotted on a time scale, in order to show the separation of the fragment from the primary body over time.

3.2 Coma size and brightness

To ensure consistent results, an estimate of the size of the inner coma of nucleus B of comet C/2011 J2 was obtained by conducting the following procedures:

- CCD images taken on each night of observation were co-added to reach a limiting magnitude of 21;
- a photometric profile was measured drawing a line across the optocenter of nucleus B, orthogonal to the PA;
- the amplitude of the light curve half-way between the peak of brightness and the sky background value was taken as the reference measure, the sky level value being determined as the median value of the entire image, not taking into account the presence of the field stars.

This procedure is similar to what happens in the dimensional measurement of the Full-Width Half-Maximum (FWHM), which describes a measurement of the width of an object or a star in a picture, when that object does not have sharp edges.

To standardize the results, they have proportionally been corrected for the distance from the Earth in AU. Since the amplitude of the curve is susceptible to variations of the *seeing* conditions, the reading error of the FWHM is estimated in ±10%. However, it should be considered that this measure was done to obtain a reproducible estimate of the average size of the coma of nucleus B over the observation period, with the aim of exploring its evolution over time, rather than to obtain a precise measure of the size of the nucleus itself, which was obviously impossible at the resolution of Earth-based images.

Moreover, we measured the ratio between the peak brightness of the primary body and that of the secondary body (in ADU) to detect possible extinction of the secondary body over time as long as it got away from the main nucleus and from the Sun. The peak values of the optocenter of the two nuclei were identified by means of aperture photometry, applying the same central window size to all images. In order to make the peak values of the two bodies comparable, they were normalized by subtraction of the sky background value in each image that was determined as for the measure of the size of the coma of nucleus B, i.e. as the median value over the entire image. To make results comparable, only the measurements taken with telescopes having aperture ≤1m with similar resolution per pixel have been considered.

3.3 Rotation period

We also run ten long series of images to determine the comet's rotation period by means of a photometric analysis of the primary nucleus (**Table 3**). To avoid random errors and the detection of false periods, the observational sessions have been spread over a very long period of about 100 days. We decided to use differential aperture photometry, with a 4-pixel radius (corresponding to about 7,000 km at the comet's distance) circular window centered on the comet's main nucleus. A concentric annulus with 80- and 120-pixels inner and outer radii, respectively, was used to detect the median sky level, far from any possible interference due to the presence of the coma or the tail. The measure of the central reading circle has been kept constant in the subsequent measures by adjusting only its radius according to the image resolution.

R-filtered images of Comet C/2011 J2
Geometric conditions during photometric sessions

Date UT	N° of images during the night	Observatory	D (AU)	R (AU)	l (°)	b (°)	Phase (°)	Colours on figures
2014-09-02.82 to 03.15	180	B13	3.5507	4.1362	13.6	37.5	12.3	black points
2014-09-28.95 to 29.06	93	B13	3.4938	4.2673	10.4	34.7	9.5	red points
2014-09-29.89 to 30.03	130	B13	3.4963	4.2724	10.3	34.6	9.4	blue points
2014-09-29.82 to 29.97	50	A12	3.4963	4.2724	10.3	34.6	9.4	violet points
2014-10-17.84 to 17.93	82	B13	3.6074	4.3673	8.3	32.7	9.3	pink points
2014-10-17.85 to 17.93	45	A12	3.6074	4.3673	8.3	32.7	9.3	maroon points
2014-10-18.77 to 18.86	50	A12	3.6176	4.3729	8.2	32.5	9.4	deep grey points
2014-10-26.72 to 26.81	40	A12	3.7094	4.4161	7.4	31.7	9.9	cyan points
2014-12-12.71 to 12.89	106	A12	4.5897	4.6802	3.2	27.1	12.1	green points
2014-12-25.75 to 25.85	63	A12	4.8794	4.7558	2.2	25.9	11.6	light grey points

D = Earth-Comet distance, **R** = Sun-Comet distance, **l** and **b** = heliocentric ecliptical longitude and latitude of the comet, **Phase** = Sun-Comet-Earth angle

Table 3

4 BRIGHTNESS AND WATER PRODUCTION

4.1 Primary nucleus

In order to derive the physical parameters of the comet C/2011 J2, we drew all published CCD magnitudes from the MPECs with their relevant astrometric positions (*Williams, 2013, 2014a, 2014b, 2014g, 2015a, 2015b*).
The resulting light curve, based on 4641 CCD observations from the MPC database, is dispersed because it resulted from the analysis of a rather faint object, and the measures came from the use of different setups; we selected only the data within 3 SD from the mean value (**Figure 5**). The trend is interpolated in the following equation:

$$m1 = H + 5\log(\Delta) + 2.5n\log(r) = 10.4 + 5\log(\Delta) + 4.2\log(r) \quad (1)$$

where H is the absolute total magnitude (defined as the total magnitude that the comet would show at a distance of 1 AU from the Sun), Δ is the distance of the comet from the Earth, and r is the heliocentric distance in AU. The residual error is of ±0.74 magnitudes.

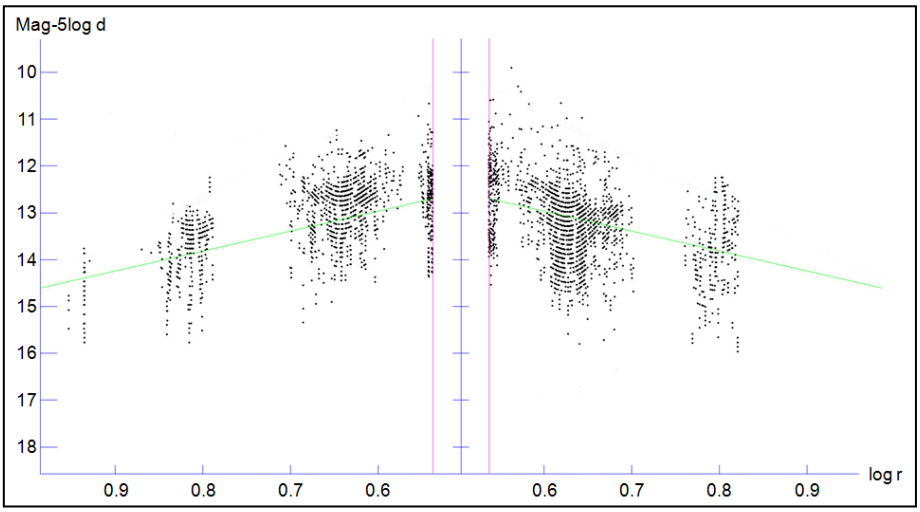

Figure 5. Plot of all CCD magnitude measures of comet C/2011 J2

The change in brightness of the comet during the apparition is therefore well determined with a total absolute magnitude H = 10.4, which appears to be low, compared to long period comets and new comets (*Hughes, 1990; Sosa, 2011*). The light curve shows a uniform trend and thus implies no evidence of outbursts. The trend is symmetrical before and after the perihelion passage, so the derived absolute heliocentric magnitude is the same before and after the perihelion.

The heliocentric magnitude trend is given by:

$$m_h = H + 2.5n\log r \quad (2)$$

where *n* is known as the photometric index, which describes variations in comet's brightness in relation to the distance *r* from the Sun. From all observations shown in Figure 5 we derived a value of *n* = 1.7; also *n* appears low if compared with that for other long period comets.

We also calculated the comet's water production rate by introducing the value of the heliocentric magnitude in the correlation found by Sosa (*Sosa, 2011*):

$$\log Q\,(H_2O) = 30.53 - 0.234\, m_{h.} \qquad (3)$$

At the perihelion, that the comet reached at 3.44 AU, log Q (H_2O) = 27.56 mol/s (about 110 kg/s).

The values of H, n and log Q are compatible with a low-activity, long-period comet.

4.2 Nucleus B

As we did for the primary nucleus, we collected all the measures of magnitude published on MPECs also for nucleus B; the resulting plot looks rather scattered ***(Figure 6)***, but the data points can be interpolated by the equation:

$$m1 = 12.5 + 5 \log(\Delta) + 6.1 \log(r) \qquad (4)$$

from which it can be calculated *n* = 2.4. The absolute total heliocentric magnitude H = 12.5 appears low, but in agreement with the values observed for the fragments of other split comets.

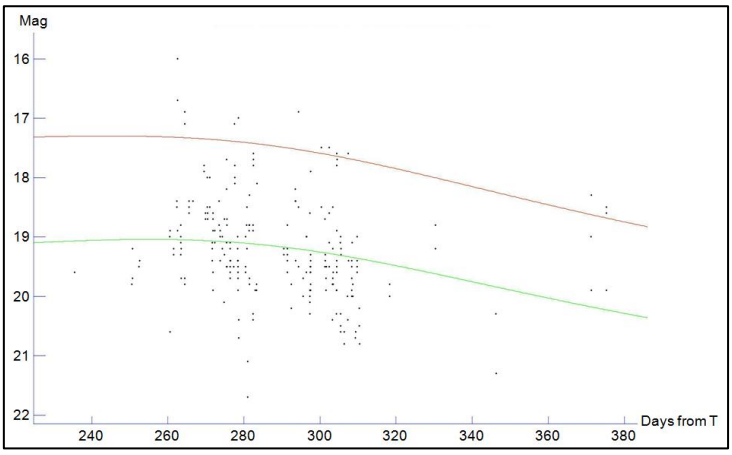

Figure 6. Plot of all magnitude measures of nucleus B

5 FRAGMENT B: MOTION, POSITION ANGLE, SIZE OF THE COMA, RELATIVE BRIGHTNESS

5.1 Progressive distance

Over the 4-month observation period, fragment B progressively departed from the main nucleus and reached an apparent distance, projected on the plane of the sky, of over 100,000 km on 11 December 2014 (our last observation date).

The apparent motion of nucleus B relative to the main nucleus projected onto the plane of the sky is shown in **Figure 7.** The diamonds indicate the measured offsets in RA and Dec in arcsec in the different observation dates. Coordinate 0,0 indicates a zero offset on the estimated date of breakup. Nucleus B showed a progressive separation towards North in Dec and towards East in RA, still following a trajectory close to the orbit of the main nucleus. The relative motion of the two bodies appears similar to that observed for other split comets for non-tidal forces (*Sekanina 1977, Sekanina 1978, Sekanina 1998, Boehnhardt 2004, Fernandez 2009*).

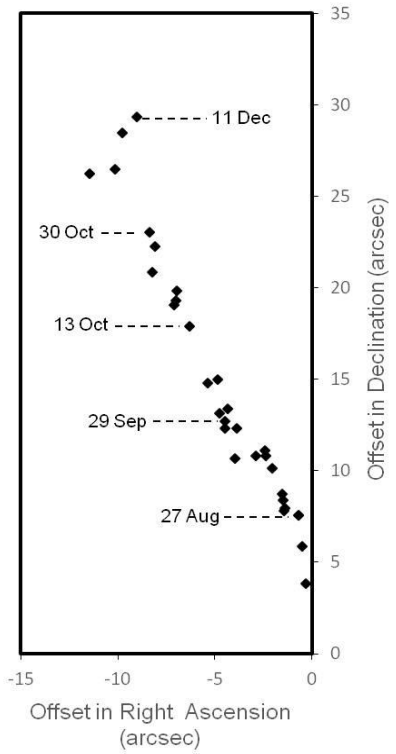

Figure 7. Apparent motion of nucleus B

Figure 8 gives the relative distance of nucleus B from the main nucleus measured in the images taken before and after the date of discovery of the breakup (27 August 2014), which is set at 0 on the x-axis. The trend looks like a parabolic function; this solid line approximates the data sets by a polynomial function, which is given as:

$$y = 2.5627x^2 + 548.78x + 16389 \quad (5)$$

where y is the relative distance in km and x is the relative days from the date of discovery.
Solution of the function shows that the distance y reaches zero for x=-35.87. This would imply that the breakup occurred approximately 36 days before the date of its discovery on 27 August, i.e. on 23 July. However, the possible measurement errors have to be considered. The functions interpolating the errors give for y=0 the following results: x=-46.5 and x=-28.51 days; we may therefore estimate that the breakup occurred within that range, i.e. between 12 July and 30 July 2014.

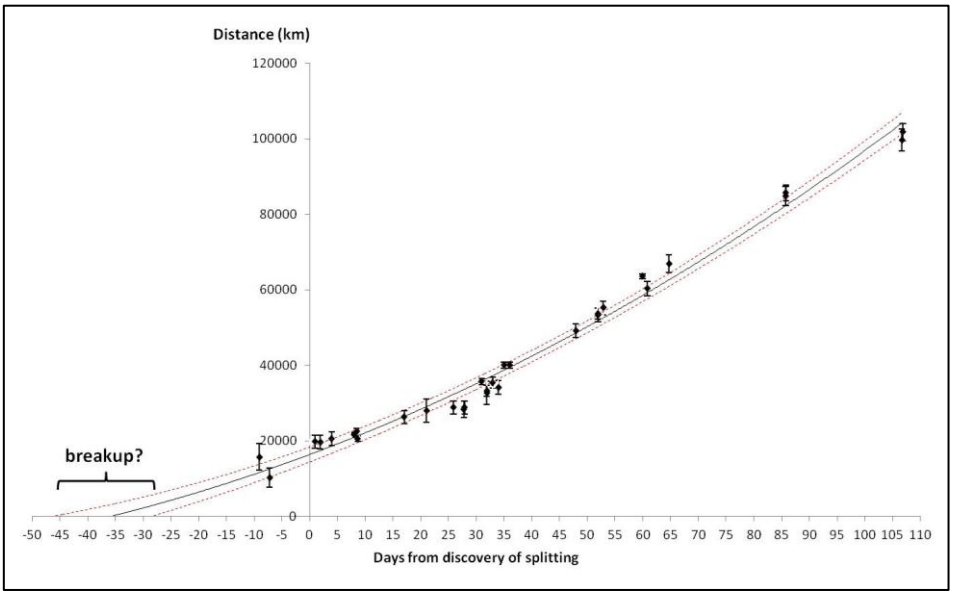

Figure 8. Relative distance of nucleus B from the main nucleus in km

Calculation of the derivative for a distance y=0 from the above equation provides that the projected separation velocity of nucleus B was $v = 4.22\, m/s$ on July 23, ranging between 3.04 m/s and 5.09 m/s considering the measurement errors described above. The separation velocity reached 12.7 m/s on 11 December.
The resulting progressive increase in the distance from the primary nucleus provides evidence that nucleus B was subjected to a constant deceleration (*Sekanina, 1977*) with respect to the motion of the primary nucleus $a = 6.87 \cdot 10^{-7} m/s^2$, corresponding to 0.0021 the Sun's gravitational acceleration at the distance of the comet of 4.0 AU ($g_{sun\ 4\ AU}$ = 3.1 * 10^{-4} m/s^2) or 0.00043 times at 1.0 AU ($g_{sun\ 1\ AU}$ = 1.58 * 10^{-3} m/s^2).

Based on the observational data collected it can be assumed that this constant deceleration motion in space is mainly due to a combined perspective effect of the orbital motions of the Earth, the main nucleus and nucleus B. However, the deceleration might also partially be attributed to uneven effects that the sun-directed outgassing from the individual components is believed to exert on their orbital momenta (*Sekanina, 1997*).
From the above considerations we also conclude that the initial separation velocity is the result of the impulse acquired by nucleus B in the course of the splitting.

5.2 Position Angle

The Position Angle of nucleus B with respect to the main nucleus over the observation period is plotted in **Figure 9a**, whereas in **Figure 9b** the same PA is plotted against the relative distance (in km) between the two bodies.
The PA of nucleus B shows slow variations over time, between 5° and 25°. However, the PA variations do not show any particular pattern of a periodicity; therefore, a hypothesis of a possible independent orbital motion cannot be confirmed.
Differently, from the second graph it appears that the PA had rapidly widened from 5° to 20° during the first days after the discovery of the breakup, whereas it stabilized around 20° at a certain point in time and remained stable irrespective of the progressive increase in the distance between the two bodies.

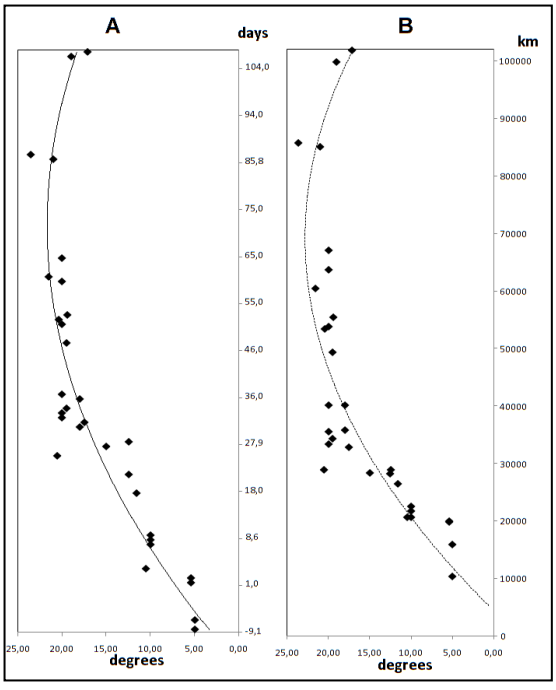

Figure 9. Position angle (PA) of nucleus B

5.3 Size of the coma

The measurement of the size of the coma of nucleus B was done on the images obtained with instruments with a diameter ≤1m in order to ensure consistent readings not affected by too large differences in spatial resolution. All co-added images useful for this work were calibrated with a limiting magnitude at 21. The

measures in the graph make a curve that does not provide an easy interpretation, and the intrinsic difficulties encountered when studying faint and diffuse objects.

The data show that, over the whole period of observation, basically there is no significant variation in the diameter of the coma of nucleus B: neither a marked enlargement, nor a clear decrease suggesting a gradual disappearance of the nucleus (**Figure 10**). The relatively stable size of the coma of nucleus B appears thus compatible with the presence of a mid- or long-lived body.

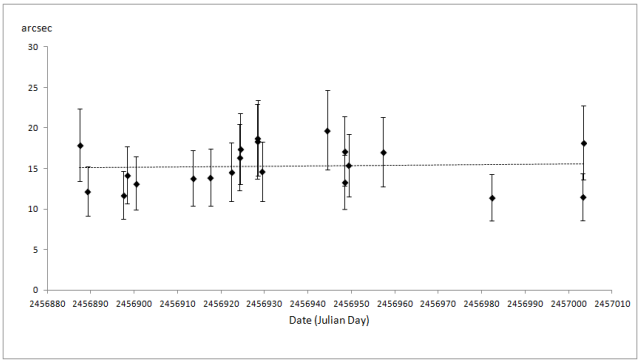

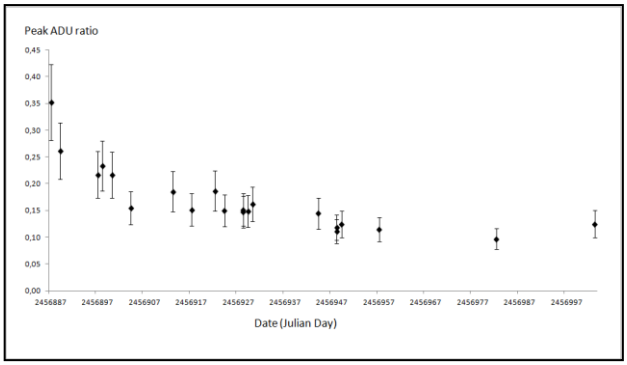

Figure 10. Size of the coma of nucleus B

Figure 11. Ratio of the peak brightness values

5.4 Brightness

To estimate the size of nucleus B relative to the main nucleus, and its possible progressive extinction over the observation period, we plotted the ratio of the luminosity peak values (in ADU) of the two bodies; the method of measurement is described in Section 3.2. Results are shown in **Figure 11**; it appears that there was a steady decrease in the brightness ratio, suggesting that a progressive extinction actually happened.
In the first few measurements, the average brightness ratio of the two optocenters is about 0.3 (nucleus B was 1.5 magnitudes fainter than the main body), whereas at the end of the observation period on December 11th the ratio was around 0.11, thus the magnitude difference rose to 2.5.
The slope of the curve suggests that nucleus B slowly faded away over time; in fact, looking at the measures of the last few observations, the reflecting surface area of the parent body resulted about 9 times larger than that of nucleus B, suggesting that the fragment had become significantly smaller.
The main nucleus and nucleus B were similarly surrounded by a faint coma; the ratio between their peak brightnesses should have made the contribution of the coma almost nil. Therefore, we hypothesize that the measure of the value of peak brightness is directly related to the size of the body surface area illuminated by the Sun. The initial ratio seems compatible with a relatively large size of nucleus B (although relatively small compared with the primary nucleus). However, it cannot be excluded that during the first weeks of observation a greater amount of residual dust following the breakup event was scattered around nucleus B, that would have raised its brightness by simply reflecting the sunlight, and thus that the first set of our measures were affected by such a phenomenon.
Given that the brightness ratio in ADU is well interpolated by one asymptotic curve to the time axis, if only the measures next to the asymptote (from JD 2456945 onwards) was taken, in order to minimize the possible confounding effect of the scattering dust, the observed extinction would appear less obvious**.**

6 PHOTOMETRY

As mentioned in paragraph 3.3, we run long series of images to determine the comet's rotation period by means of a photometric analysis of the parent nucleus after the discovery of its fragmentation. The observing sessions were performed in 9 dates (**Table 3**; **Figure 12**), spread over a period as long as about 100 days. We analyzed differential photometry using calibrated stars in the image field of view to minimize the effects due to seeing and atmospheric variations and obtain better-calibrated measures.

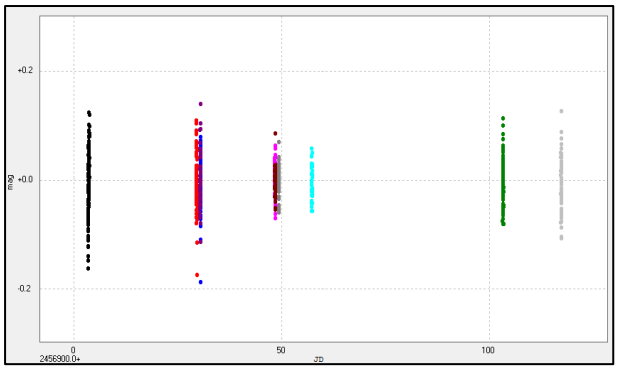

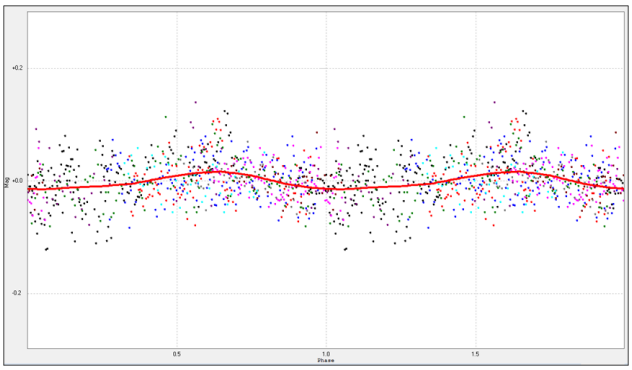

Figure 12. Plot of all photometry sessions

Figure 13. Light curve of the primary body of comet C/2011 J2

A complete analysis of all this data has identified a light curve within the area covered by the photometric analysis, showing the highest probability for a possible period of 0.19 ± 0.002 days (4.56 ± 0.05 hours) with a small, but detectable 0.004 magnitude variation (**Figure 13**).

Indeed, we should not expect significant variations in magnitude for a small body at a distance of 4.0 AU, unless there are large diurnal variations due to the presence of active sources modulated by the rotation period. The size of our photometric window included a wide area around the nucleus, so that the measure of the magnitude would have taken into account the presence of such phenomena. The study of the inner coma morphology did not show any presence of features related to emitting areas. The small variations in the photometric measurements could therefore be due to an area on the nucleus exposed because of the breakup; this area should show a different albedo than that observed on any other part of the surface of the primary nucleus, and such as to determine small magnitude variations, that show an apparent period because of the rotation of the nucleus.

To assess and validate our results found we also did the following: we tested all our photometric observations using the methods of Bloomfield (*Bloomfield, 1986*), ANOVA (*Schwarzenberg-Czerny, 1996*), DFT Deeming (*Deeming, 1975*) and PDM (*Stellingwerf, 1978*), and they all provided consistent values, with the most significant probability for values between 4.2 and 4.6h.

The light curve looks repetitive in the long run and therefore it is realistic to think that it is due to a phenomenology related to the nucleus, probably induced by the fragmentation. The periodogram showing this light curve has been obtained by means of the Date Compensated Discrete Fourier Transform method (DCDFT), as seen in **Figure 14** (*Ferraz-Mello, 1981*). This method calculates the power spectrum of unequally spaced data using a so called 'date-compensated' discrete Fourier transform. This transform is defined so as to include the uneven spacing of the dates of observation and weighting of the corresponding data.

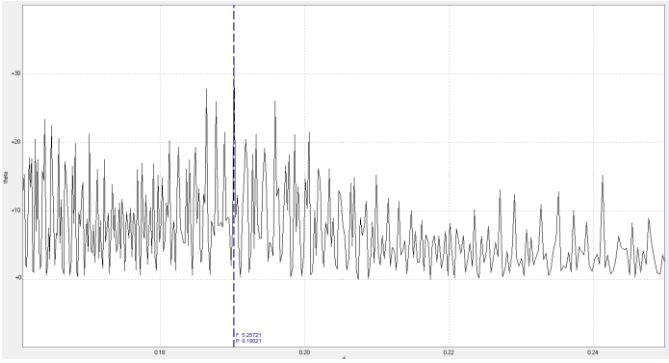

Figure 14. Analysis of the photometric measurements

7 DYNAMICAL AND STRUCTURAL ANALYSIS

7.1 Possible scenarios

There are three possible scenarios to explain the breakup event of comet C/2011 J2: collisional impacts, rotational disruption and sublimation due to the rise of surface temperature.

We first eliminate collisional impacts from the possible breakup scenario. Since impacts produce ejecta with a broad range of velocities (*Housen and Holsapple 2011*), such a different velocity spectrum should have been observed as well as a noticeable increase in the comet's brightness due to the impact. However, the observations indicate that nucleus B departed from the main nucleus with a relatively small velocity $v = 4.22\ \mathrm{m/s}$ (3.04 m/s < v < 5.09 m/s considering the measurement errors, as shown in section 5.1) projected on the sky plane.

Rotational breakup may be a possible explanation for the breakup event of C/2011 J2. The estimated rotation period is 4.56 ± 0.05 hours, which can cause a cometary nucleus to fail structurally. If a body is spherical and cohesionless, the spin period condition at which surface materials on the equator are shed is characterized as a function of the bulk density (*Hirabayashi and Scheeres, 2014b*). If the bulk density is 2000 kg/m^3, this critical spin period is 2.3 hours, which is comparable to the spin barrier of rubble pile asteroids (*Pravec et al. 2007*). If the bulk density is 500 kg/m^3, a typical value for cometary nucleus, T=4.67 hours. Therefore, the rotation of the nucleus of C/2011 J2 is faster than this critical value. If the body is elongated, the critical spin period becomes slower (*Hirabayashi et al., 2014a*). This implies that the main nucleus should be close to its rotational failure and needs certain strength to avoid catastrophic failure.

Sublimation due to the rise of the surface temperature may be another possibility. Using the similar technique by *Jewitt et al.* (2014), we found that the equilibrium temperature at 4.1 AU is about 160 K, leading to internal pressure of ~0.01 Pa. This value may be lower than the reported strength of the nucleus of 67P/Churyumov-Gerasimenko, which is ~15 Pa (*Groussin et al. 2015*). However, since the nucleus of C/2011 J2, whose eccentricity is 1.0, may not come closer to the Sun often, there may be substantially weak regions in the body. Thus, sublimation pressure may be able to cause a mass of the nucleus to depart from the progenitor body.

However, we also consider that sublimation-driven activity can be induced by fast rotation as well. Sublimation-driven activity is typically observed after cometary bodies pass their perihelion passages. A remarkable example is the seasonal activity of main belt comet 324P/La Sagra, whose eccentricity is 0.154 (*Hsieh and Sheppard, 2015*). More interestingly, main belt comet 133P/Elst-Pizarro was reported to have a fast rotation period of 3.71 hours while having seasonal activities (*Hsieh et al., 2010*). This report infers that fast rotation and sublimation may be highly correlated with each other to enhance cometary activities (*Hsieh, personal communication, 2015*). These cases can be considered to be analogous to the breakup event of C/2011 J2, which was first observed at a heliocentric distance of 4.1 AU on July 23, 2014, after its perihelion on December 25, 2013.

In the next section, hypothesizing that rotational effects play a crucial role in the breakup event of C/2011 J2, we make a simple model for giving constraints on the mechanical properties of the material of this comet.

7.2 Consideration of rotational breakup

7.2.1 Assumptions

We develop a rotational model for the breakup event between the main nucleus and nucleus B to place constraints on the physical properties of this system. Assumptions are made to simplify our discussion.

- First, we assume that the progenitor nucleus is a uniformly distributed biaxial ellipsoid.
- Second, the progenitor body is considered to be rotating uniformly and to keep its state during the breakup event.
- Third, our model assumes that after the breakup of the progenitor body, nucleus B is a massless point, and the main nucleus is a biaxial ellipsoid. This assumption is reasonable as the photometric measurements showed that nucleus B was about between 1.5 and 2.5 magnitudes fainter than the main nucleus, corresponding to a brightness of about three to nine times lower (see Section 5.4).
- Fourth, the ejection of nucleus B comes from structural failure of the progenitor body, and the initial separation velocity ranging between 3.04 m/s and 5.09 m/s (Figure 8) solely results from its fast rotation. In other words, the progenitor body fails structurally, and then nucleus B is ejected from the progenitor body with the same velocity as the surface velocity.

- Last, we assume the bulk density of the nuclei to be 500 kg/m^3, which is based on the current observations of 67P/Churyumov-Gerasimenko (*Preusker et al. 2015*).

In the following discussion, we only consider the motion in the projected sky plane. Thus, the obtained results here show the lower bounds for the actual values.

7.2.2 Modeling

Before discussing our model, we introduce three parameters to describe elliptic integrals as we consider the progenitor body to be a biaxial ellipsoid. Given the ratio of the semi-minor axis to the semi-major axis, β, which is later called the aspect ratio, we define the elliptic integral parameters (*Hirabayashi, 2014c*):

$$A_0 = \beta^2 \iiint \frac{du}{(\beta^2+u)\sqrt{(1+u)}}, \tag{6}$$

$$A_x = \beta^2 \iiint \frac{du}{(\beta^2+u)(1+u)\sqrt{(1+u)}}, \tag{7}$$

$$A_z = \beta^2 \iiint \frac{du}{(\beta^2+u)^2\sqrt{(1+u)}}, \tag{8}$$

We model dynamical motion and structural mechanics of the system by using simple shapes (**Figure 15**). Again, the progenitor body is assumed to be a biaxial ellipsoid rotating uniformly. Once the progenitor body fails structurally, it splits into the main nucleus and nucleus B. Since the mass of nucleus B is assumed to be negligible, we also consider that the sizes of the progenitor body and the main nucleus are not different. Because of this, the spin rate of the main body is assumed to be the same as that of the progenitor body. Note that if the mass of nucleus B is not small enough, these assumptions are no longer appropriate in our model as angular momentum transfer becomes significant and more complex dynamics occurs (*Jacobson and Scheeres, 2011*). Hirabayashi et al. (*Hirabayashi, 2014a*) considered such a separation problem under the assumption that the total energy remains constant though it is necessary to develop a further sophisticated model.

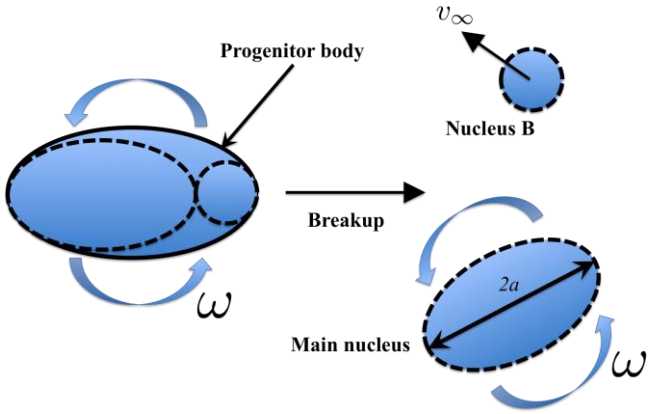

Figure 15. Breakup model

The orbital motion of the main nucleus and nucleus B is described by using energy conservation of the two-body problem. We write the semi-major axis of the main nucleus a as

$$a^2 = \frac{v_\infty^2}{2\pi\rho G(-A_0+A_x)+\omega^2} \tag{9}$$

where ρ is the bulk density, v_∞ is the initial separation velocity and ω is the spin rate of the main nucleus at which nucleus B is ejected. This form is obtained on the assumption that the proto-body of nucleus B is resting on the tip of the biaxial progenitor body.

Plastic structure analysis is used to model the failure condition of the progenitor body. Specifically, in our model, structural failure of the progenitor body occurs when the majority of the stress field reaches the yield. To describe the stress field, we use the averaged stress over the volume (*Holsapple, 2007*):

$$\sigma_x = (\rho\omega^2 - 2\,\pi\rho^2 G\, A_x)\frac{a^2}{5}, \tag{10}$$

$$\sigma_z = -2\,\pi\rho^2 G\, A_z \frac{a^2\beta^2}{5}, \tag{11}$$

where σ_x and σ_z are the principal components of the averaged stress along the semi-major axis and the semi-minor axis, respectively. The yield condition is described by using the Mohr-Coulomb yield criterion (*Chen and Han, 1989*):

$$Y \geq Y_{cr} = \frac{\sigma_x - \sigma_z}{2}\sec\phi + \frac{\sigma_x + \sigma_z}{2}\tan\phi, \tag{12}$$

where Y is cohesive strength, Y_{cr} is its critical value, and ϕ is a friction angle. Here, we assume ϕ to be 35 degrees (*Lambe and Whitman, 1969*). Substituting equations (9) through (11) into equation (12) yields

$$Y_{cr} = \frac{\sec\phi + \tan\phi}{10}\frac{(\omega^2 - 2\pi\rho G A_x)\rho v_\infty^2}{2\,\pi\rho G\,(-A_0 + A_x) + \omega^2} + \frac{\sec\phi - \tan\phi}{5}\frac{\pi\rho^2 G\, A_z\beta^2 v_\infty^2}{2\,\pi\rho G\,(-A_0 + A_x) + \omega^2}. \tag{13}$$

This form is useful because Y_{cr} is directly dependent on v_∞ and ω.

It is important to note that a uniformly distributed spherical body spinning fast may fail from the middle region, which causes similarly sized components (*Hirabayashi et al., 2014a; Hirabayashi, 2015*). To have a small component departing from the progenitor body, the progenitor body may have weak surface region (*Hirabayashi and Scheers, 2014b*), which may support the sublimation-driven activity scenario. However, we avoid a sophisticated model in this study, as our purpose is to simplify our analysis to only focus on the separation of the breakup event.

7.2.3 Results

We first calculate the range of β from equation (6). Given the bulk density as 500 kg/m^3, since the denominator must be positive, we obtain it as $\beta < 0.675$. This result implies that the progenitor body and thus the main nucleus may have highly elongated bodies. Such elongated bodies may be common as dwarf planet Haumea's aspect ratio is 0.5 (*Rabinowitz, 2006)*.

From equation (13), we then obtain the semi-major axis and the cohesive strength as a function of the aspect ratio. Since the progenitor body can be considered to fail at the observed spin period, the ranges of v_∞ and ω provide possible range of these quantities. **Figure 16** shows the range of the semi-major axis (**16a**) and that of the cohesive strength (**16b**). The dashed and dotted lines describe the cases for initial dispersion velocities of 3.04 m/s and 5.09 m/s, respectively, while the solid line shows that of 4.22 m/s. The shaded area is the available region of these quantities. As the aspect ratio becomes zero, these quantities decrease. Taking the zero aspect ratio, we obtain the lowest bounds for these quantities. The semi-major axis should be larger than 8 km, and the cohesive strength should be higher than 0.9 kPa.

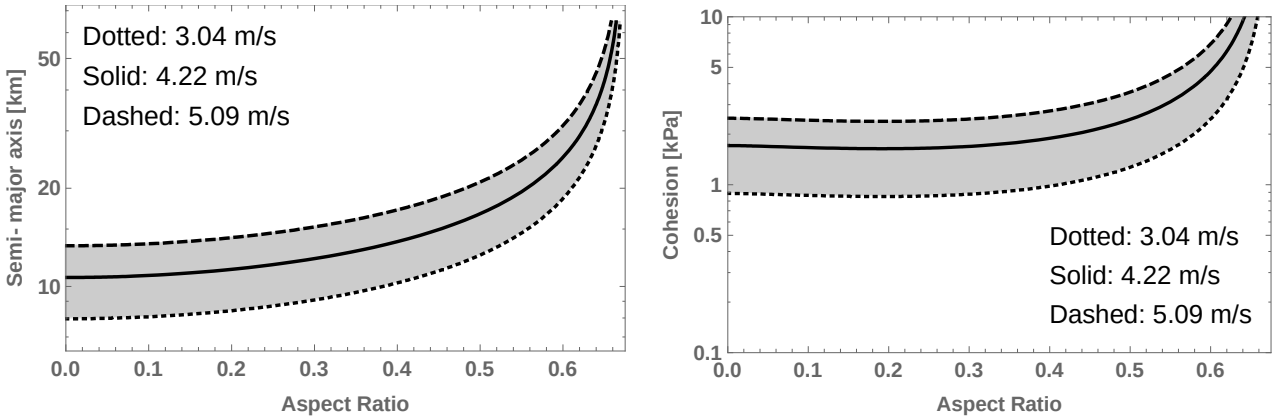

Figure 16. Semi-major axis (a) and cohesion (b) of the pristine nucleus of comet C/2011 J2

Given the brightness ratio between the main nucleus and nucleus B, which implies the relation of their sizes, we may estimate that the size of nucleus B was negligible compared with that of the parent body.

Our results show that the size of the progenitor body and, again, the main nucleus should be at least on the order of tens of kilometers. This lower limit may be consistent with earlier studies reporting the sizes of cometary nuclei. The radius of the nucleus of C/1729 P1 is considered to be on the order of 100 km in radius (*Sagan and Druyan, 1997*). Also, the reported nucleus of comet Hale-Bopp ranges between 13.5 km and 21 km (*Weaver et al., 1997*). More recently, radii of 20 and 28 km, respectively, have been estimated for the nuclei of comets C/2007 D3 (LINEAR) and C/2010 S1 (LINEAR) (*Ivanova et al., 2015*). In addition, it was reported that the observed size distribution of solar system bodies orbiting beyond Neptune is predominantly on the order of tens of kilometers (*Bernstein et al., 2004; Pan and Sari, 2005*).

8 CONCLUSIONS

After the discovery of a first breakup event on 27 August 2014, we followed comet C/2011 J2 for about 120 days, until 11 December 2014, and observed the presence of two fragments, named B and C, respectively. While the latter was very faint and short-lived, fragment B remained persistently observable throughout the entire observation period. This allowed the collection, exchange and pooling of many images by several professional and amateur observatories in the world. The analysis of such a significant amount of data enabled us to outline a thorough description of the phenomena resulting from the splitting which is hardly attainable by a single observatory, and to a sufficient extent that we could hypothesize its causes.

The observations of comet C/2001 J2 showed values of absolute total magnitude (H = 10.4), photometric index (n = 1.7) and water production (110 kg/s) that characterize it as belonging to the species of low-activity, new or long-period comets.

The projected separation velocity of nucleus B from the primary body was 4.22 m/s at the time of the breakup. This separation velocity is the result of the impulse acquired by nucleus B in the course of the splitting. Ivanova et al. found a value of 4.9 m/s, which corresponds only to the average speed between September 18 and October 10, 2014 (*Ivanova, 2016)*; although this value is in good agreement with our measurements in those dates, it does not take into account the acceleration of nucleus B.

According to our calculations, the separation velocity reached 12.7 m/s at the end of the observation period, showing a trend typical of a constant acceleration motion. Sekanina (*Sekanina, 2014*) reported a modeling of the companion's motion relative to the primary nucleus of C/2011 J2 based on positional offsets derived from the astrometry published on MPECs (*Green, 2014*), suggesting that the companion was a strongly decelerating fragment (about 0.0008 the Sun's gravitational acceleration) of a fairly short lifetime (estimated at 20-40 days at 1 AU from the Sun). Our data basically confirm that nucleus B was a strongly decelerating fragment, although at a different value than that proposed by Sekanina. According to our measurements, nucleus B was subjected to a constant deceleration $a = 6.87 \cdot 10^{-7} m/s^2$ with respect to the primary body, corresponding to 0.0021 the Sun's gravitational acceleration at the distance of the comet.

In the same CBET Sekanina stated that separation of fragment B from the parent body had occurred with a sub-meter velocity some 2 weeks after perihelion, in early January 2014 (*Sekanina, 2014*). According to our

estimates, the breakup should have occurred between 12 July and 30 July 2014, i.e. six months later than when hypothesized by Sekanina. Furthermore, no evidence of nucleus B could be found in earlier CCD images at our disposal (2 April, 11 and 14 June, 1 July 2014).

Nucleus B remained persistently visible throughout the 4-month observation period, but we could no longer detect it in images taken with a magnitude 21 limit to this purpose in September 2015, i.e. about 14 months after the C/2011 J2 nucleus splitting. The endurance of the fragment estimated by Ivanova (*Ivanova, 2016*) applying the Sekanina equation (*Sekanina 1977, 1982*) is clearly not consistent with the fact that nucleus B was still observable over 150 days after the splitting.

Having detected by means of photometry of the main nucleus a possible rotation period of 4.56h, and assuming that the ejection velocity of nucleus B was the same as the measured projected separation velocity of 4.22 m/s), the primary nucleus should have been relatively large in size to have such a rotation speed in its equatorial zone. In fact, our results show that the size of the progenitor body and of the residual main nucleus should be at least on the order of tens of kilometers.

Our observational data, combined with the physical data found on other comets by probes or other authors, have enabled us to develop a rotational model suitable to determine the shape and size of comet C/2011 J2 and to explain the fragmentation event. In particular, the progenitor body -and thus the residual main nucleus- should have biaxial ellipsoid elongated bodies, with a ratio of the semi-minor axis to the semi-major axis $\beta < 0.675$, a cohesive strength higher than 0.9 kPa, and a semi-major axis $a > 8$ km.

The size of the semi-major axis is in agreement with that found by other means ($R \leq 9$ km) by Ivanova (*Ivanova, 2016*) applying the equation proposed by Jewitt (*Jewitt, 1991*), assuming the presence of a spherical nucleus.

As far as the mechanism that caused the splitting of the comet's nucleus, rotational disruption appears the most reasonable explanation. Nucleus C has most likely broken up from the main nucleus with the same mechanism.

This model can be used for the study of other split comets for which the main physical parameters, such as the rotation period and the ejection speed of the secondary bodies, are available.

9 ACKNOWLEDGEMENTS

We thank:

- Emilio Molinari, director of TNG; Marco Pedani and the staff of Telescopio Nazionale Galileo (Canarias) for the great help provided in shooting the images with the TNG.
- Stefano Benetti at INAF Astronomical Observatory of Padova (Italy) for the great help allocating observational time on this comet at the Schmidt telescope.
- François Colas, IMCCE, Observatoire de Paris (France), for the help during the access to the 1-m telescope at the Pic du Midi.
- David Jewitt at UCLA for his useful comments on the observational part discussed in this paper.
- Lino Colombo at IIS Inveruno (Italy) for the useful mathematical discussions.
- Paolo Bacci, Centro Astronomico Libbiano Peccioli (Italy); Luca Buzzi,Osservatorio Astronomico Campo dei Fiori Varese (Italy); Peter Carson, Leigh on See (Essex, UK); Roberto Haver, Osservatorio di Frasso Sabino (Italy) for providing useful CCD images.

This research is partly based on observations made with DOLoRes@TNG (Telescopio Nazionale Galileo at Canarias) and the Copernico and Schmidt telescopes (Asiago, Italy) of the INAF - Osservatorio Astronomico di Padova.

This research has also made use of public images of the Liverpool Telescope (Canarias), and of the LCOGT public Archive, which is operated by the California Institute of Technology, under contract with the Las Cumbres Observatory.

REFERENCES

1. Altenhoff W.J. et al. (2009). Why did Comet 17P/Holmes burst out? Nucleus splitting or delayed sublimation? A&A 495, 975-978. DOI 10.1051/0004-6361:200810458
2. Bernstein G.M. et al. (2004). The size distribution of Trans-Neptunian bodies. AJ 128, 1364-1390. DOI 10.1086/422919
3. Bloomfield P. (1986). Fourier analysis of time series: an introduction. Wily ed., New York.
4. Boehnhardt H. (2004). Split Comets. In: Comets II, 301-316. The University of Arizona Press, Tucson.
5. Chen W. F. and Han D. J. (1988). Plasticity for structural engineers. Springer Verlag, New York.
6. Deeming T.J. (1975). Fourier analysis with unequally-spaced data. Ap&SS 36, 137-158. DOI 10.1007/BF00681947
7. Fernandez Y.R. (2009). That's the way the comet crumbles: Splitting Jupiter-family comets. P&SS 57, 1218-1227. DOI 10.1016/j.pss.2009.01.003
8. Ferraz-Mello S. (1981). Estimation of periods from unequally spaced observations. AJ 86, 619-624. DOI 10.1086/112924
9. Green D.W.E. (2014). [IAUC] CBET 3979: 20140919: COMET C/2011 J2 (LINEAR)
10. Groussin O. et al. (2015). Gravitational slopes, geomorphology, and material strengths of the nucleus of comet 67P/Churyumov-Gerasimenko from OSIRIS observations. A&A, 583, A32. DOI 10.1051/0004-6361/201526379
11. Hirabayashi M. et al. (2014a). Constraints on the physical properties of main belt comet P/2013 R3 from its breakup event. ApJ Lett. 789, L12. DOI 10.1088/2041-8205/789/1/L12
12. Hirabayashi M. and Scheeres D.J. (2014b). Analysis of asteroid (216) Kleopatra using dynamical and structural constraints. ApJ, 780, 160. DOI 10.1088/0004-673X/780/2/160
13. Hirabayashi M. (2014c). Structural failure of two-density-layer cohesionless biaxial ellipsoids. Icar. 236, 178-180. DOI 10.1016/j.icarus.2014.02.024
14. Hirabayashi M. (2015a). Failure modes and conditions of a cohesive, spherical body due to YORP spin-up. MNRAS 454, 2249-2257. DOI 10.1093/mnras/stv2017
15. Hirabayashi et al. (2015b). Internal structure of asteroids having surface shedding due to rotational instability. ApJ 808, 63. DOI 10.1088/0004-673X/808/1/63
16. Holsapple K.A. (2007). Spin limits of Solar System bodies: from the small fast-rotators to 2003 EL61. Icar. 187, 500-509. DOI 10.1016/j.icarus.2006.08.012
17. Housen K.R and Holsapple K.A. (2011). Ejecta from Impact Craters. Icar. 211, 856-875. DOI .1016/j.icarus.2010.09.017
18. Hsieh H. et al. (2010). The return of activity in main-belt comet 133P/Elst-Pizarro. MNRAS 403, 363-377. DOI 10.1111/j.1365-2966.2009.16120.x
19. Hsieh H. and Sheppard S. (2015). The Reactivation of Main-Belt Comet 324P/La Sagra (P/2010 R2). MNRAS Lett., 454, L81. DOI 10.1093/mnras/slv125
20. Hughes D.W. (1990). Cometary absolute magnitudes - their significance and distribution. In: Asteroids, Comets, Meteors III. Eds. Lagerkvist C.I. Rickman H., Lindblad B.A. and Lindgren M. University of Uppsala Reprocentralen, 327-342.
21. Ivanova O. et al. (2015). Observations of Comets C/2007 D1 (LINEAR), C/2007 D3 (LINEAR), C/2010 G3 (WISE), C/2010 S1 (LINEAR), and C/2012 K6 (McNaught) at large heliocentric distances. Icar. 258, 28-36. DOI 10.1016/j.icarus.2015.06.026
22. Ivanova, O. et al. (2016). Comet C/2011 J2 (LINEAR): Photometry and stellar transit. Planetary and Space Science. DOI 10.1016/j.pss.2016.01.005i
23. Jewitt D.C. (1991). Cometary photometry. In: Comets in the post-Halley era. Kluwer,Dordrecht, 1, pp. 19–65
24. Jewitt D.C. et al. (2014). Disintegrating asteroid P/2013 R3. ApJ Lett. 784, L8. DOI 10.1088/2041-8205/784/1/L8
25. Jacobson S.A. and Scheeres D.J. (2011). Dynamics of rotationally fissioned asteroids: source of observed small asteroid systems. Icar. 214, 161-178. DOI 10.1016/j.icarus.2011.04.009
26. Lambe T.W. and Whitman V.W. (1969). Soil mechanics. John Wiley & Sons, New York.
27. Larson S. and Sekanina Z. (1984). Near nucleus study of comet Halley. JPL Cometary Astrometry, 14-20.

28. Manzini F. et al. (2001). Comet Hale-Bopp shells expansion: a CCD study. EM&P 87, 73-85. DOI 10.1023/A:1017597207597

29. Manzini F. et al. (2007). Comet Ikeya-Zhang (C/2002 C1): determination of the rotation period from observations of morphological structures. EM&P 100, 1-16. DOI 10.1007/s11038-005-9062-6

30. Manzini F. et al. (2011). Comet Machholz (C/2004 Q2): morphological structures in the inner coma and rotation parameters. Ap&SS. DOI 10.1007/s10509-011-0866-8.

31. Manzini F. et al. (2014). Comet McNaught (260P/2012 K2): spin axis orientation and rotation period. Astrophys Space Sci. DOI 10.1007/s10509-014-1854-6.

32. Pan M. and Sari R. (2005) Shaping the Kuiper belt size distribution by shattering large but strengthless bodies. Icarus 173, 342-348. DOI 10.1016/J.icarus.2004.09.004

33. Pravec P., Harris A.W and Warner B.D. (2007). NEA rotations and binaries. Proc. IAU Symposium 236, 2006.

34. Preusker F. et al. (2015). Shape model, reference system definition, and cartographic mapping standards for comet 67P/Churyumov-Gerasimenko–Stereo-photogrammetric analysis of Rosetta/OSRIS image data. A&A 583, A33. DOI 10.1051/0004-6361/201526349

35. Rabinowitz D.L. et al. (2006). Photometric observations constraining the size, shape, and albedo of 2003 EL61, a rapidly rotating, Pluto-sized object in the Kuiper belt. ApJ 639, 1283-1251. DOI 10.1086/499575

36. Sagan C. and Druyan A. (1997). Comets. Ballantine eds. New York.

37. Schwarz G. et al. (1997). Comet Hale-Bopp: evolution of jets and shells during March 1997. EM&P 78, 189-195. DOI 10.1023/A:1006240714442

38. Schwarzenberg-Czerny A. (1996). Fast and statistically optimal period search in uneven symplex observations. ApJ Lett. 460, L107-110. DOI 10.1086/309985

39. Sekanina Z. (1977). Relative motions of fragments of the split comets I. A new approach. Icar. 30, 574-594. DOI 10.1016/0019-1035(77)90111-7

40. Sekanina Z. (1978). Relative motions of fragments of the split comets II. Separation velocities and differential decelerations for extensively observed comets. Icar. 33, 173-185. DOI 10.1016/0019-1035(78)90031-3

41. Sekanina Z. (1982) The problem of split comets in review. In: Comets (L. L. Wilkening, ed.), pp. 251-287. University of Arizona, Tucson.

42. Sekanina Z. and Yeomans D.K. (1985) Orbital motion, nucleus precession, and splitting of periodic Comet Brooks 2. AJ. 90, 2335–2352. DOI 10.1086/113939

43. Sekanina Z. (1997). The problem of split comets revisited. A&A Lett. 318: L5-L8. Bibcode 1997A&A…318L…5S

44. Sekanina Z. (1998) A double nucleus of Comet Evans-Drinkwater (C/1996 J1). A&A Lett. 339, L25-L28. Bibcode 1998A&A…339L..25S

45. Sekanina Z., et al. (2002) Recurring outbursts and nuclear fragmentation of Comet C/2001 A2 (LINEAR). ApJ, 572, 679-684. DOI 10.1086/340284

46. Sekanina Z. (2005). Comet 73P/Schwassmann-Wachmann: Nucleus fragmentation, its light-curve signature, and close approach to Earth in 2006. ICQ 27, 225-240. Bibcode 2005ICQ….27..225S

47. Sekanina Z. (2014). Comet C/2011 J2 (LINEAR). CBET 3986. Bibcode 2014CBET.3986….1S

48. Sosa et al. (2011). Masses of long-period comets derived from non-gravitational effects - analysis of the computed results and the consistency and reliability of the non-gravitational parameters. MNRAS 416, 767-782. DOI 10.1111/j.1365-2966.2011.19111.x

49. Spahr T.B., Williams G.V. (2014). MPC 89407 and MPC 89408

50. Stellingwerf R.F. (1978). Period determination using phase dispersion minimization. ApJ 224, 953-960. DOI 10.1086/156444

51. Weaver H.A. et al. (1997). The activity and size of the nucleus of comet Hale-Bopp (C/1995 O1). Science 275, 1900-1904. DOI 10.1126/science.275.5308.1900

52. Williams G.V. (2011), Observations and orbits of comets, MPEC 2011-J31, 2011

53. Williams G.V. (2013), Observations and orbits of comets, MPEC 2013-P52, 2013

54. Williams G.V. (2014a, b, c, d, e, g), Observations and orbits of comets, MPEC 2014-E86, 2014a; MPEC 2014-P41, 2014b; MPEC 2014-R69, 2014c; MPEC 2014-R70, 2014d; MPEC 2014-S34, 2014e; MPEC 2014-U124, 2014g

55. Williams G.V. (2014f), Comet C/2011 J2-C, MPEC 2014-W30, 2014f.

56. Williams G.V.(2015a, b), Observations and orbits of comets, MPEC 2015-E14, 2015a; MPEC 2015-S97, 2015b

FIGURE CAPTIONS

Figure 1. Discovery of the splitting of comet C/2011 J2.
Image of the discovery of nucleus B (27 August 2014), resulting from a total exposure time of 40 minutes as sum of single frames. The coma of the main nucleus appears evenly diffuse, almost circular, with a diameter of 50". Fragment B was at a 7.6" distance from the primary nucleus, corresponding to about 19700 km. A faint tail develops at PA 20°. Images taken with the 0.4-m Cassegrain telescope at the Stazione Astronomica di Sozzago (Italy).

Figure 2. Enhancement of coma details
Images taken with the 3.6-m TNG (Telescopio Nazionale Galileo) telescope at Canarias on 25th October 2015. The motion of the comet was tracked, so stars appears as trails; North is up, East to the left. The color image is 2x enlarged to show the presence of fragment C near the primary nucleus. The bar indicates 30 arcsec as measured in the two images (corresponding to about 80500 km at the comet distance).

Figure 3. Enhancement of details: radial gradient filter
When images are difficult to read, they can be processed with different filters to put details into evidence; in this specific case the coma is faint and there is no apparent tail (left); treatment with a radial gradient filter shows very well nucleus B and its morphological characteristics that would otherwise remain hidden within the coma of the main body (right). Images taken on August 27.9, 2014 with the 0.4-m Cassegrain telescope at the Stazione Astronomica di Sozzago (Italy). North is up, East left.

Figure 4. Measurement method of the positions of nucleus B
The original image was 2x re-sampled and then submitted to polar coordinates transformation centered on the central peak of brightness of the primary body. The photometric profile 1 (below graph) is drawn parallel to the horizontal axis and crossing the bright area corresponding to nucleus B to identify the position angle of its optocenter with respect to the 0° angle of the polar rotation. The photometric profile 2 (right graph) is drawn orthogonally to the first across nucleus B to measure its separation in pixels from the x-axis (i.e. from the optocenter of the main nucleus). On the x-axis, in A the θ angle and in B the distance from the optocenter in pixels, respectively. On the y-axis the brightness value in ADU. Image taken at Faulkes LCOGT North 2-m telescope; date of observation: 02 September 2014, JD 2456932.4437.

Figure 5. Plot of all CCD magnitude measures of comet C/2011 J2
All 4641 CCD photometric measures published on MPECs were added to analyze the luminosity trend of comet C/2011 J2 and to derive its absolute magnitude. The x-axis is the log of the comet's distance from the Sun; The y-axis gives the values of the observed magnitude minus 5 log Δ (where Δ is the distance of the comet from the Earth). The green line shows the interpolating linear trend.

Figure 6. Plot of all magnitude measures of nucleus B
The plot presents all MPEC published magnitude measures on B-body of comet C/2011 J2. On the x-axis are days from the time T of perihelion. The green line show the best interpolating trend.

Figure 7. Apparent motion of nucleus B
Projected motion of nucleus B relative to the parent nucleus after the estimated date of breakup (23 July 2014). The diamonds indicate the measured offsets in RA and Dec in arcsec in the different observation dates. Coordinate 0,0 indicates the zero offset on the date of breakup. Dotted marks indicate some of the observation dates. North is up and East is left.

Figure 8. Relative distance of nucleus B from the main nucleus in km
Relative distance of nucleus B from the main nucleus measured in the available images taken before and after the date of discovery of the breakup (27 August 2014), which is set at 0 on the x-axis. The diamonds are the measured distances in km on each observation date. The solid line is the trend line. The trend line indicates that the relative distance y reaches zero 35.87 days before the discovery, on JD 2456861.59 (23 July 2014). The dotted lines are the functions interpolating the measurement errors, that reach zero for x = -46.5 and x = -28.51 days, respectively. The breakup should have occurred within this time interval, i.e. between 12 July and 30 July 2014.

Figure 9. Position angle (PA) of nucleus B
Plot of the Position Angle (in degrees) of the fragment B relative to the primary nucleus during the observation period (A: PA values in the different observation dates. B: PA relative to the distance between the two bodies in km).

Figure 10. Size of the coma of nucleus B
Measurements of the size of the coma of fragment B; the reference measure was taken half-way between the peak of brightness of the fragment B and the sky background value. The graph show the measurements obtained with telescopes of a diameter <1m. Data have been normalized for the distance from the Earth in AU. The error bars show the size of the reading error of the FWHM, estimated at ±10%. Dotted line is the linear trend.

Figure 11. Ratio of the peak brightness values
Ratio of the peak value in ADU of fragment B on the primary nucleus, measured directly on the CCD images and calibrated for the sky background. The graph shows a consistent reduction over time, indicating a progressive extinction of nucleus B. The error bars show the size of the reading error, estimated at ±20%.

Figure 12. Plot of all photometry sessions
Plot of all photometry measurements taken on the primary nucleus since JD 2456903.32; the dot colors are explained in Table 3.

Figure 13. Light curve of the primary body of comet C/2011 J2
All photometry measurements of nucleus A of comet c/2011j2, taken over an observation period as long as 100 days, are displayed in this phased graph which shows a clear repetitive pattern suggesting a possible period of 0.1903 days; the dot colors are explained in Table 3.

Figure 14. Analysis of the photometric measurements
All photometry measurements of nucleus A, analyzed with the DCDFT method (Ferraz-Mello), show a peak corresponding to a possible period of 0.1903 days.

Figure 15. Breakup model
Breakup model. Initially, the biaxial progenitor body is rotating uniformly. Then, after failure occurs, the body is separated into two components: one being the main nucleus, which is a biaxial ellipsoid, and the other being nucleus B, which is a point mass. Here, from our observations, we assume that the mass of nucleus B is negligible compared to that of the main nucleus. We referred to Jacobson and Scheeres (2011) to illustrate our failure model.

Figure 16. Semi-major axis (a) and cohesion (b) of the pristine body of comet C/2011 J2
Semi-major axis (a) and cohesion (b) as a function of the aspect ratio β (where β is the ratio of the semi-minor axis to the semi-major axis). The dotted, solid and dashed lines show the cases for initial dispersion velocities of 3.04, 4.22 and 5.09 m/s, respectively.